DOI: 10.21917/ijivp.2011.0029

FABRIC DEFECT DETECTION USING STEERABLE PYRAMID

S. Mythili
Department of Computer Science & Engineering, United Institute of Technology, Tamil Nadu, India
E-mail: mythili@uit.ac.in

Abstract

In this paper, a novel idea is proposed for fabric defect detection. Defects are detected in the fabric using steerable pyramid along with a defect detection algorithm. Various steerable pyramid of four size 256*256, 128*128, 64*64, 32*32 and with four orientation bands 0^0,45^0, 90^0, 135^0 are used. Utilizing a Steerable pyramid proved adequate in the representation of fabric images in multi-scale and multi-orientations; thus allowing defect detection algorithms to run more effectively. Defect detection algorithm identifies and locates the imperfection in the defective sample using the statistics mean and standard deviation. This statistics represents the relative amount of intensity in the texture and is sufficient to measure defects in the current model .The obtained result are compared with the existing methods wavelet based system and with Gaussian and Laplacian pyramid .

Keywords:

Fabric Automatic Visual Inspection, Steerable Pyramid, Feature Extractor, Defect Detector

1. INTRODUCTION

In modern textile industry, Fabric Automatic Visual Inspection (FAVI) system is an attractive alternative to human vision inspection. Based on advances in computer technology, image processing and pattern recognition, FAVI system can provide reliable, objective and stable performance on fabric defects inspection [3], [4], [15]. These systems do not suffer the drawbacks of human visual inspection, such as fatigue, boredom, or inattentiveness. Automated systems are able to inspect fabric in a continuous manner without pause. The goal of this paper is to find a feasible algorithm to base an automated inspection system to identify and locate the imperfections in periodic textured surface [16].

In many image processing applications, an image is decomposed into a set of subbands, and the information within each subband is processed more or less of that in other subbands. This process is known as multi-scale analysis [6] and can be used in texture analysis [7] since it decomposes the texture across several different scales, which serves to greatly improve analysis. The texture can now be inspected at various scales such that a feature vector comprised of significant features at each scale can be created and used as a base for defect classification.

In this regard, a bank of gabor filters [12] at suitable orientations and scales would be inconvenient. An orthonormal wavelet [13] representation suffers from a lack of translation-invariance, which is likely to cause artifacts [8]. Thus, we chose to use a "steerable pyramid" [5], [6], [17], since this transform has nice reconstruction properties (specifically, it is a tight frame), in addition to properties of translation-invariance and rotation- invariance and applying an efficient algorithm results in significant level of defect detection [9]. An unsolved problem is not only to deal with detection, but also with location. Essentially in solving this problem, a mark is made on the defect to find its position.

Organization of the paper is as follows: Chapter 2 background knowledge of steerable pyramid is described. Chapter 3 describes the proposed fabric defect detection system. Implementation details and experimental analysis are summarized in Chapter 4. Finally Chapter 5 includes the concluding remarks.

2. BACKGROUND KNOWLEDGE

2.1 STEERABLE PYRAMID

To identify and locate detection in periodic textures surface, the proposed method adopt the steerable pyramid transform [18]. Like the Laplacian pyramid [14], this transform decomposes the image into several spatial frequency bands. In addition, it further divides each frequency band into a set of orientation bands. . The result is a detailed analysis of the image for defect detection.

2.2 STEERABLE PYRAMID GENERATION

The system diagram of steerable pyramid for a Kth stage is shown in Fig.1. The system is divided into two parts, analysis and synthesis. On the left side of the diagram is analysis part. The image is decomposed into lowpass and highpass subbands, using steerable filters L0 and H0. The lowpass band continues to break down into a set of bandpass subbands B0, …, Bk and lower lowpass subband L1. The lower lowpass subband is subsampled by a factor of 2 along the x and y directions. Repeating the shaded area provides the recursive structure.

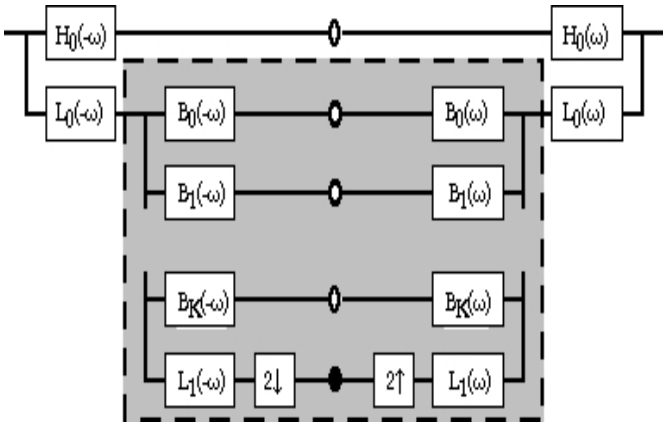

Fig.1. System Diagram for a *K*th Derivative Steerable Pyramid

On the other hand, the right side of the diagram is synthesis part. The synthesized image is reconstructed by upsampling the lower lowpass subband by the factor of 2 and adding up with the set of bandpass subbands and the highpass subbands.

2.3 BASE FILTER IN THE EXPERIMENT

We chose to use the same complex steerable filter which is used in texture synthesis application to build the steerable pyramid [10]. The filters used in this transformation are polar-separable in the Fourier domain.

2.3.1. The Lowpass Filters:

The magnitude response of an ideal low pass filter allows low frequencies π/4in the pass band to pass, whereas the higher frequencies π/2 in the stopband are blocked. The steerable low pass filter is given

$$L(r,\theta) = \begin{cases} 2\cos\left(\frac{\pi}{2}\log_2\left(\frac{4r}{\pi}\right)\right), & \frac{\pi}{4} < r < \frac{\pi}{2} \\ 2, & r \le \frac{\pi}{4} \\ 0, & r \ge \frac{\pi}{2} \end{cases}, \quad (1)$$

$\frac{\pi}{4} < r < \frac{\pi}{2}$ are the band limits. r, θ are the polar co-ordinates. The lowpass band is subsampled by a factor of two along both axes (and thus requires amplitude of two). Unlike conventional orthogonal wavelet decompositions, the subsampling does not produce aliasing artifacts, as the support of the lowpass filter $L(r,\theta)$ obeys the Nyquist sampling criterion. The recursive procedure is initialized by splitting the input image into lowpass and highpass portions, using the following filters:

$$L_0(r,\theta) = L\left(\frac{r}{2},\theta\right)\Big/2 \quad (2)$$

$$H_0(r,\theta) = H\left(\frac{r}{2},\theta\right). \quad (3)$$

2.3.2. The Highpass Filters:

The high pass filter allows high frequency above π/2 and rejects the frequency lesser than π/4

$$H(r) = \begin{cases} \cos\left(\frac{\pi}{2}\log_2\left(\frac{2r}{\pi}\right)\right), & \frac{\pi}{4} < r < \frac{\pi}{2} \\ 1, & r \ge \frac{\pi}{2} \\ 0, & r \le \frac{\pi}{4} \end{cases}. \quad (4)$$

2.3.3. The Steerable Band Pass Filters:

The k directional bandpass filters used in the iterated stages are given by

$$B_k(r,\theta) = H(r)G_k(\theta), \qquad k \in [0, k-1] \quad (5)$$

$$G_k(\theta) = \begin{cases} \alpha_K\left[\cos\left(\theta - \frac{\pi k}{K}\right)\right]^{K-1}, & \left|\theta - \frac{\pi k}{K}\right| < \frac{\pi}{2} \\ 0, & otherwise \end{cases} \quad (6)$$

$$\alpha_K = 2^{K-1}\frac{(k-1)!}{\sqrt{K[2(K-1)]!}} \quad (7)$$

r, θ are the polar co-ordinates, K is the number of scales in the pyramid, k is the number of orientation bands, $\theta = \tan^{-1}(v/u)$ is the angular variable in frequency space.

3. METHODOLOGY AND SYSTEM DESCRIPTION

3.1 OVERVIEW OF THE METHOD

In this paper, the defect detection system is divided into two parts (1) feature extractor and (2) defect detector. Feature extractor is used to calculate the reference statistics (mean and standard deviations) of the non-defective fabric. Defect detector is used to detect and locate the imperfections in the defective fabrics (same pattern of non-defective fabric) with the help of the reference statistics.

The initial step of the feature extractor and defect detector is used to represent non-defective and defective samples in Steerable pyramid form. Complex "analytic" filters [10] are used to build the pyramid; hence coefficients of Steerable pyramid are complex (a + bi). Then magnitude of the complex pyramid is divided by resized low-pass residual image of the pyramid. This normalized magnitude is known as contrast units; which is one type of texture features. Important structural information is obtained from these contrast units which are helpful to locate defects in the texture.

The first stage of the algorithm is the feature extractor. In the feature extraction scheme, the mean and standard deviations are computed for each orientation at various scales of Steerable pyramid (non-defective sample). This computed values are used as reference statistics for defect detector stage. Mean and standard deviations represents the relative amount of intensity in the texture.

The second stage of the algorithm is the defect detector. The first step is to find the magnitude difference between features; for each pixel or location in different orientations and scales of pyramid, the features of the sample under inspection with those of the reference statistics mean. In order to reduce noise, when difference between features is below threshold value; difference is set as zero. Then information of each scale with different orientations is combined together. The result of this contains the information on the likely defective areas. Finally the information coming from different scales are combined together to account for defects detected at different scales. The last stage corresponds to the binarization to provide an image where local defects appear segmented from the fabric (background).

The method presented in this algorithm must meet three requirements. Firstly, it has to enhance changes in the descriptors, which may correspond to a defect in such a way that a binarization makes possible the segmentation of defective areas from the textured background. Secondly, the process must integrate defects captured in different orientations and scales of the pyramids into a single binary map as the output with the location of defects. Thirdly, the procedure must be automatic, robust, versatile and easily adaptable to a variety of regular textures of different materials.

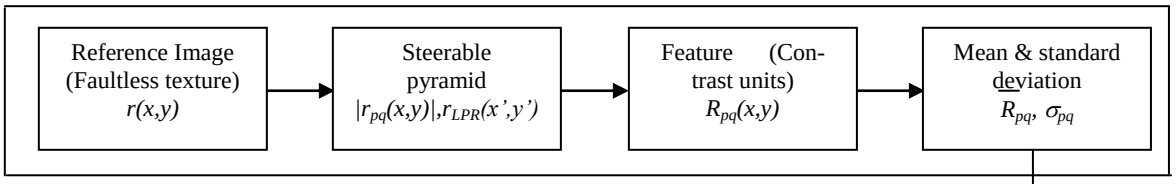

Fig.2(a) Feature Extractor

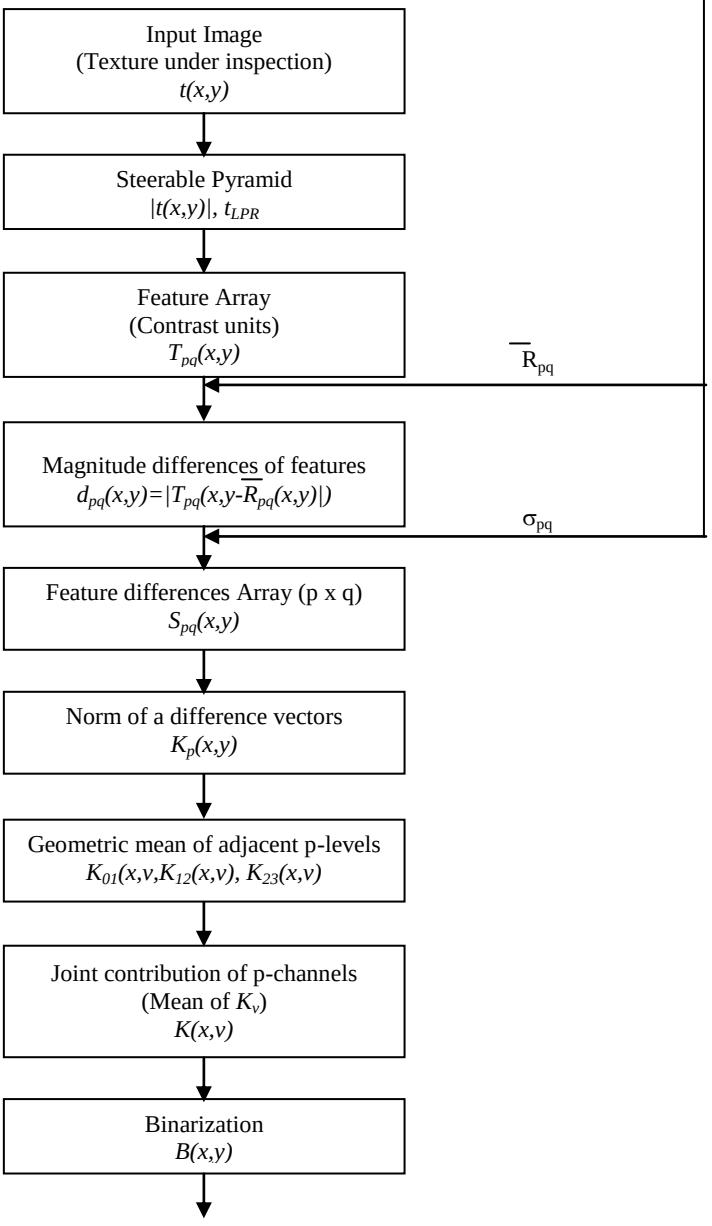

Fig.2(b) Defect Detector

Fig.2. Block Diagram of Defect Detection System

3.2 FEATURE EXTRACTOR

Given a non-defective fabric, the goal is to extract the statistics features mean and standard deviation which is used as a reference to identify the defect in the fabric. The algorithm for feature is described below:

Step1: Decompose the image into multiscale and multiorientation using steerable pyramid. Let p=0, 1, 2, 3 represent scaling by 2p and q = 0, 1, 2, 3 represent the four orientation $q\pi/4$ .The coarser approximation obtained after

the fourth decimation is the low pass residual image $r_{LPR}(x', y')$.

In the second step, our texture descriptors are obtained by expressing the module of the complex details $|r_{pq}(x, y)|$, that we call the filtered image, in contrast units. This is accomplished by dividing every |rpq (x, y)|, by the resized low-pass residual image $r_{LPR}(x', y')$.Thus, the set {p, q} of features $R_{pq}(x, y)$ are given for each pixel (x, y) by the expression,

$$R_{pq}(x,y)=\frac{\left|r_{pq}(x,y)\right|}{r_{LPR}(x',y')}, \tag{8}$$

With

$$x'=1+I\left(\frac{x-1}{2^p}\right), \qquad y'=1+I\left(\frac{y-1}{2^p}\right), \tag{9}$$

where function $I(z)$ means the integer part of argument z.

Step 2: The mean value (over all the pixels) of each R_{pq} and the standard deviation σ_{pq} are calculated by standard expressions where Np 2 is the number of pixels of the filtered image in the resolution level p.

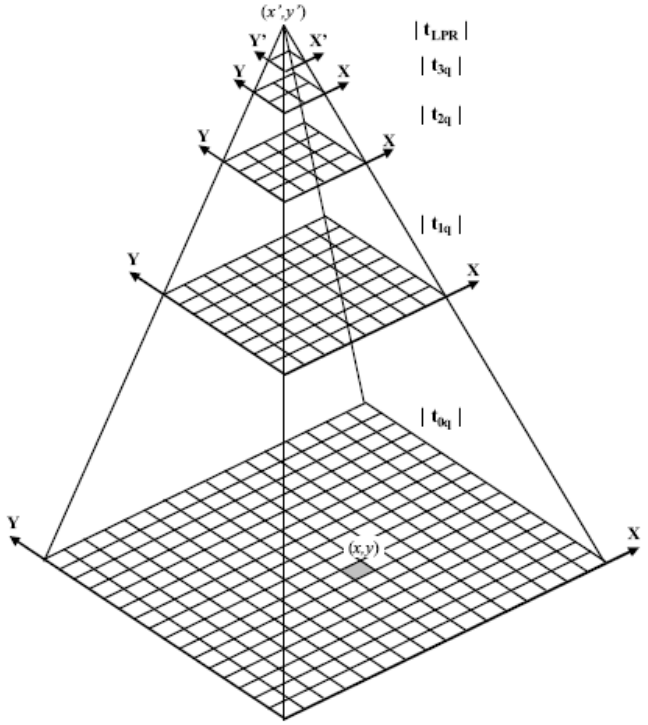

Fig.3. Partial representation of the pyramid distribution used to express the filtered images $|r_{pq}(x, y)|$ in contrast units by dividing by the low-pass residual $r_{LPR}(x', y')$ [13]

The two sets of sixteen (4x4) values $\{R_{pq}\}$ and $\{\sigma_{pq}\}$ are the reference entry to the main procedure on the right of the scheme in Fig.2 [13].

$$\overline{R_{pq}}=\sum_{x=1}^{N_p}\sum_{y=1}^{N_q}R_{pq}(x,y), \tag{10}$$

$$\sigma_{pq}=\sum_{x=1}^{N_p}\sum_{y=1}^{N_p}R_{pq}(x,y). \tag{11}$$

3.3 DEFECT DETECTOR

This section describes the procedure we propose for defect detection in regular textures:

Step 1: It starts with an image of the sample to inspect $t(x,y)$. The complex steerable pyramid is constructed for this test sample. The values for p and q are considered as discusses in previous section. After fourth decimation, the resulted coarser approximation is $t_{LPR}(x,y)$ which is a low pass residual image.

By means of expressing the module of the complex details $|t_{pq}(x, y)|$, the texture descriptors are gathered in this step. This is called as filtered image.

This is realized by splitting each $|t_{pq}(x, y)|$ with the help of resized low-pass residual image t_{LPR}. Therefore, the set $\{p, q\}$ of features $T_{pq}(x, y)$ are provided for every pixel (x, y) as below

$$T_{pq}(x,y)=\frac{\left|t_{pq}(x,y)\right|}{\left|t_{LPR}(x',y')\right|}. \tag{12}$$

Step 2: This step is to compare, for each pixel or location, the features of the sample under study with those of the reference. The closer the values, the higher the likelihood of it coinciding with the prototype, and conversely, the larger the difference the higher the probability of there being a defect. Thus, we calculate, for each level p and orientation q, the magnitude of the difference between contrast units of the sample under analysis and the prototype defect-free sample

$$d_{pq}=\left|T_{pq}(x,y)-\overline{R_{pq}}(x,y)\right|. \tag{13}$$

Step 3: In order to reduce noise, for each pixel we set as zero those differences $d_{pq}(x, y)$ below a threshold; i.e. for those values with a high likelihood of being like the prototype. We consider a standard thresholding operation given by the expression:

$$S_{pq}(x,y)=\begin{cases} d_{pq}(x,y), & d_{pq}(x,y)\geq \tau\sigma_{pq} \\ 0, & otherwise \end{cases}, \tag{14}$$

where the threshold is proportional to the standard deviation σ_{pq} calculated from the reference feature array $R_{pq}(x, y)$. We take a fairly standard constant value $\tau = 3$ according to a low risk criterion: only points with differences above three times the standard deviation are eligible as defects, which strongly reduces the probability of misclassifying points of the background (regular texture) as defective areas. The resulting array of the thresholded feature differences is represented by $S_{pq}(x, y)$ in the diagram in Fig.2(b).

Step 4: For each scale level p and for every pixel (x, y), a vector of four components $S_p^{xy} = \{(S_p^q)_q\}$ with $q = 0\ldots3$ can be built. Each component of the vector is S_p^{xy} defined by $(S_p^{xy})_q \equiv S_{pq}(x, y)$ and coincides with the thresholded fea-

ture difference of pixel (x, y) in the scale level p and orientation q. In the next stage an array $K_p(x, y)$ is calculated for each scale level p with the norm of vectors S_p^{xy}, that is,

$$K_p(x,y) = \left\| S_p^{xy} \right\| = \left\{ \sum_{q=0}^{3} \left[S_{pq}(x,y) \right] \right\}^{1/2} \quad (15)$$

The definition of K_p, i.e., the norm of the feature difference vector is a common metric used in standard clustering algorithms for segmentation. According to Eq.(15), the array $K_p(x, y)$ concentrates the information on the likely defective areas obtained in the four orientations $q = 0\ldots3$ in a single array for the scale level p. Thus, the result of this stage is a set of four images $K_p(x, y)$ with $p = 0\ldots3$.

Step 5: In the next two stages we combine the information coming from the four different resolution levels p. To this end the resized version of each $K_p(x, y)$ array is prepared. In order to avoid false alarms we consider that a defect must appear in at least two adjacent resolution levels. As a simple way to implement a logic "and", assuming that $K_p(x, y)$ is proportional to the probability of there being a defect, we then calculate the geometric means of every pair of adjacent levels given by the formulas:

$$K_{01}(x,y) = \left[K_0(x,y).K_1(x,y) \right]^{1/2}, \quad (16)$$

$$K_{12}(x,y) = \left[K_1(x,y).K_2(x,y) \right]^{1/2}, \quad (17)$$

$$K_{23}(x,y) = \left[K_2(x,y).K_3(x,y) \right]^{1/2}, \quad (18)$$

This operation reduces false alarms yet preserves most of the defective areas. Now we combine the resulting $K_{01}(x, y)$, $K_{12}(x,y)$ and $K_{23}(x, y)$ in a logic "or", simply as the arithmetic mean, to account for defects detected at different scales:

$$K(x,y) = \frac{1}{3}\left(K_{01}(x,y) + K_{12}(x,y) + K_{23}(x,y) \right). \quad (19)$$

The array $K(x,y)$ contains the joint contribution of the sixteen pq-channels.

Step 6: The last stage corresponds to the binarization of $K(x,y)$ to provide an image $B(x,y)$ where local defects (objects) appear segmented from the regular texture (background).This is achieved by thresholding $K(x,y)$. Values below the threshold are considered as belonging to the background and values above the threshold are considered as belonging to defective areas.

This threshold value is not critical and can be estimated in different ways. One possible way is to calibrate the system at the beginning of the process by applying the procedure to an additional piece of faultless texture whose image would be the input image $t_0(x,y)$.In this case the obtained array $K_0(x,y)$ should contain very low values. An estimation of the threshold U as with Ko being the mean value of $K_o(x,y)$, σ_o its standard deviation and ρ a standard constant of value $\rho = 3$, provides an appropriate threshold value for binarization. Alternatively, a simpler way is to calculate which is proportional to the mean value of the sixteen standard deviations σ_{pq} with a constant of proportionality equal to a standard value, for example, $\rho = 3$.

4. EXPERIMENTATION RESULTS AND COMPARISON

Experimentation of algorithm is done using twill fabric images of standard size 256*256 obtained from Miquel Rallo [13]. If the twill fabric images are not of standard size, then nearest neighbor interpolation method is adopted to resize the input fabric images to standard size. The Steerable pyramid used for experimentation is of four levels and four orientations for both feature extractor and defect detector.

4.1 EXPERIMENTATION RESULTS: FEATURE EXTRACTOR

The algorithm uses the input of non defective twill fabric image shown in Fig.4. From the input image, Steerable pyramid of four levels of size 256*256, 128*128, 64*64, 32*32 and each having four orientation bands at 0^0,45^0, 90^0,135^0 are constructed using filter Eqs.(1-7).The results are shown in Fig.5. The mean and standard deviations of contrast units for different scales and orientations are calculated using Eqs.(10 &11) and tabulated in Table.1.

Fig.4. Non-Defective Twill Fabric Image

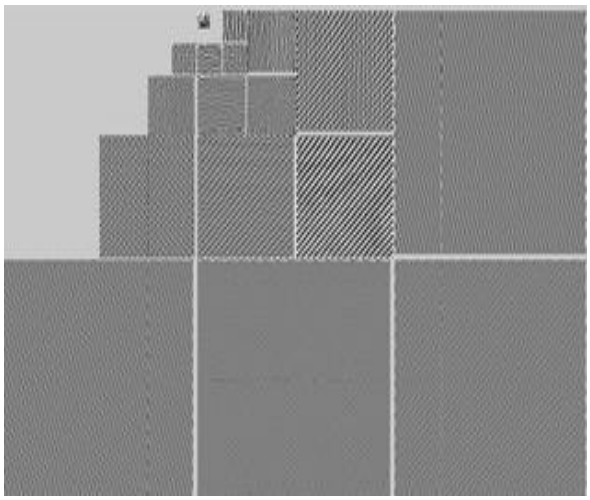

Fig.5. Non-Defective Fabric; Steerabl Pyramid A 4 - scale, 4-Orientation Band Pass Images at 0 0,450, 900 and 1350 and the Final Lowpass Image

Table.1. Reference Statistics of Non-Defective Twill Fabric Image from Steerable Transform

Orientation		0^o	45^o	90^o	135^0
Scale 1 (256*256)	μ	0.00086848	0.00051954	0.00032498	0.00065957
	σ	0.00015788	9.4511e-005	0.00016146	8.4423e-005
Scale 2 (128*128)	μ	0.0053868	0.0092205	0.003312	0.0027172
	σ	0.0011287	0.0011248	0.0005661	0.0010408
Scale 3 (64* 64)	μ	0.016737	0.041634	0.015206	0.0074612
	σ	0.0024913	0.0019255	0.0019255	0.001587
Scale 4 (32*32)	μ	0.015566	0.0099739	0.01074	0.010997
	σ	0.0044265	0.0033038	0.0031363	0.003556

4.2 EXPERIMENTATION RESULTS: DEFECT DETECTOR

The defect detector algorithm is experimented with defective twill fabric images displaying variety of shapes: line, spot, band, ladder, hole, etc as defects. These defects are caused by missing or broken yarns or by changes in tension during production in the loom. The results are discussed as follows

Fig.6 shows a sample of twill fabric image containing thin-place defect. The defect appears as a band in the central part of the image and is caused by a lower density of filling yarns in this band. Corresponding Steerable pyramid representation is shown in Fig.7. The defective layers for each pyramid levels p = 0...3 is shown in Figs.8(a)-(d). Then geometric means of every pair of adjacent levels i.e. levels one and two, two and three, three and four are calculated and shown in Fig.9(a) to (c). Finally, the joint contribution of all the geometric means are shown in Fig.9(d). The binary image, which constitutes the output image, is shown in Fig.9(e). The defective band at the center is correctly located in defective fabric image as shown in Fig.9(f).

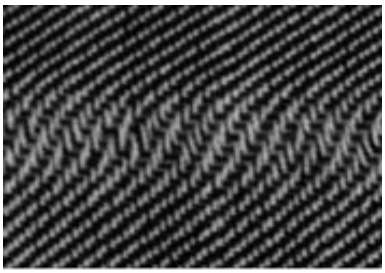

Fig.6. Thin-Place Effect in a Twill Fabric Image

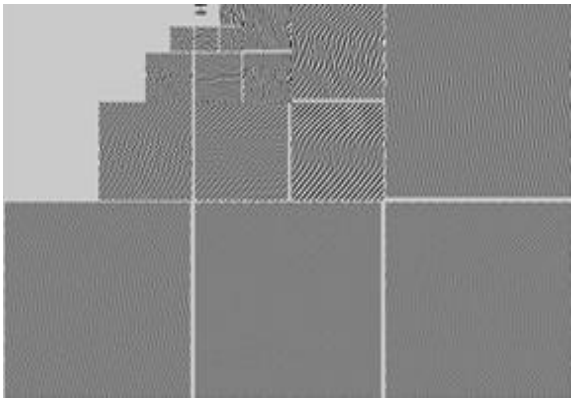

Fig.7. Defective Fabric; Steerable Pyramid a 4-Scale, 4-Orientation Band Pass Images at 0o, 450, 900 and 1350 and the Final Lowpass Image

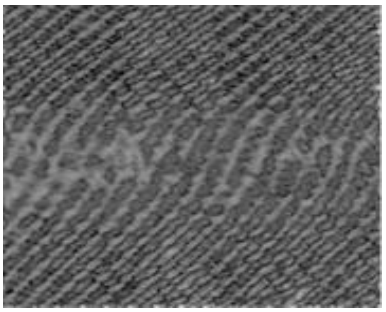

8(a) p=0

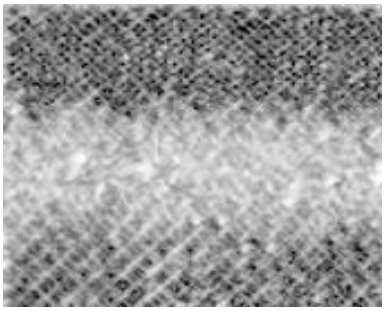

8(b) p=1

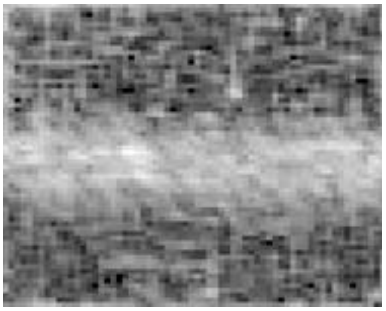

8(c) p=2

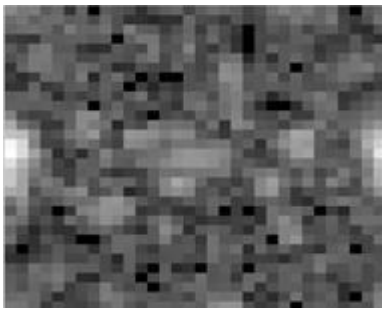

8(d) p=3

Fig.8. (a)-(d) Defective Layers for the Pyramid Levels (p)

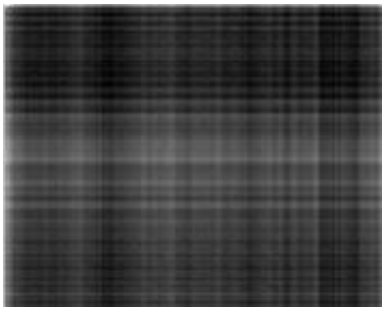

9(a)

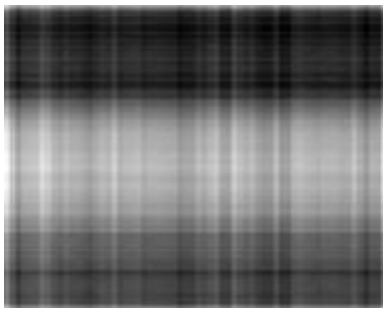

9(b)

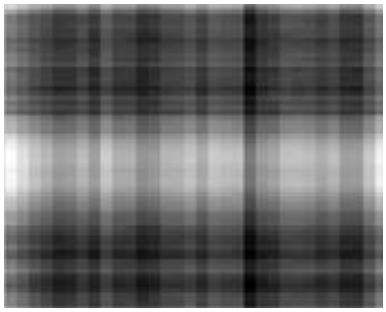

9(c)

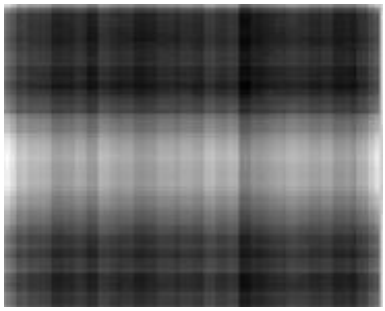

9(d)

9(e)

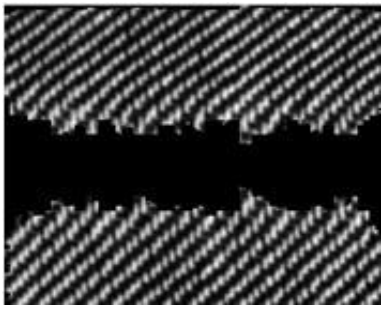

9(f)

Fig.9. (a) to (c) Geometric Means of Every Pair of Adjacent Levels; (d) Joint Contribution of the all Scales; (e) Binary Output Image; (f) Defect Location in Twill Fabric

The image of twill fabric with defects along a line due to missing yarn and double yarn are shown in Fig10(a) and Fig.11(a) respectively. In both cases, defective part is correctly located and corresponding binary image is as shown in Fig.10(b) and Fig.11(b) respectively. The twill fabric image with down heddle defect is shown in Fig.12(a). The defect due to down heddle is a dotted distribution and difficult to locate, our algorithm works well in detecting these dotted distributions shown in Fig.12(b).

10(a)

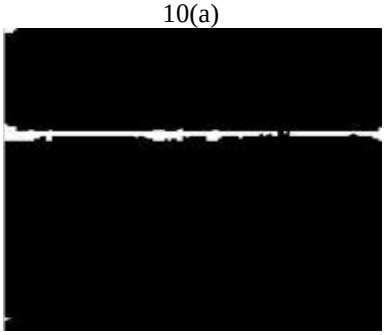

10(b)

Fig.10. (a) Twill Fabric with Missing Yarn Defect; 10(b) Output Binary Image

11(a)

11(b)

Fig.11. (a) Twill Fabric with Double Yarn Defect; 11(b) Output Binary Image

12(a)

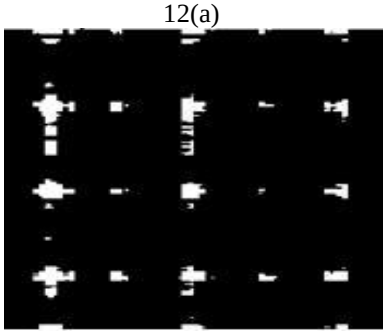

12(b)

Fig.12. (a) Twill Fabric with Down Heddle Defect; 12(b) Output Binary Image

The defect detection algorithm is tested for an image and its translated scaled version as shown in Fig.13(a) and Fig.13(b). The algorithm does not identify any defect from the two images which proves the translation invariance and scaled invariance of the Steerable pyramid. This helps us to get the robust result for slight movement of the camera. The proposed method is superior to gray level co-occurrence matrices method for defect detection [1] where it is not translation invariant.

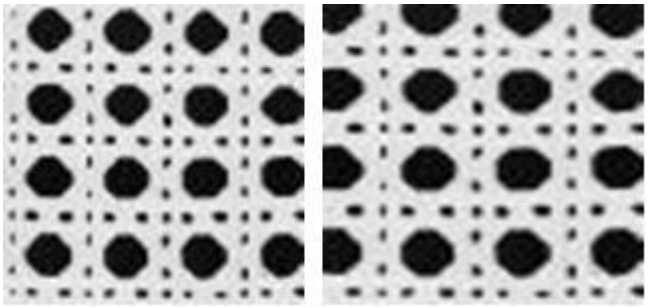

(a) (b)

Fig.13. (a) Bordtaz Texture; 13(b) Translated Bordtaz Texture

4.3 COMPARISON WITH WAVELET BASED TECHNIQUE

Our defect detection result for Twill fabric image with down heddle defect is compared with the result obtained in the paper [13]. Comparison shows that Wavelet based technique find difficulty in detecting and discriminating some dots from background. Only 8 out of 15 are detected by applying the general method (Fig.14(a)). Our proposed method allows us to locate all the defects (15 out of 15).

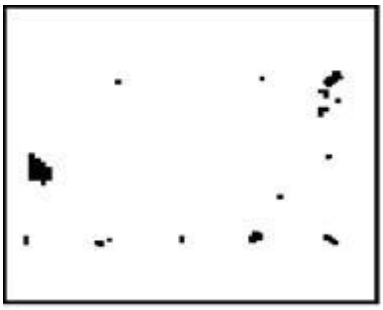

14(a)

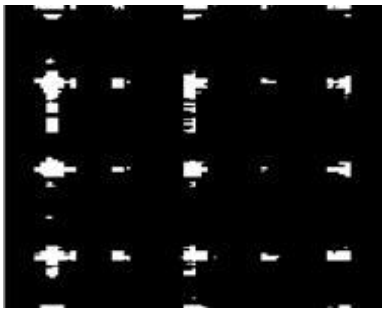

14(b)

Fig.14. Comparison of twill fabric images with down heddle defect

4.4 COMPARISON WITH GAUSSIAN AND LAPLACIAN PYRAMID

In addition to Steerable pyramids, the algorithm is tested with Gaussian pyramid Fig.15(a) and Laplacian pyramid Fig. 15(b). Experimentation clearly shows that those pyramids are capable only for partially identifying thin place defect of twill fabric image shown in Fig.16. and are not capable to identify other defects for example down heddle defects.

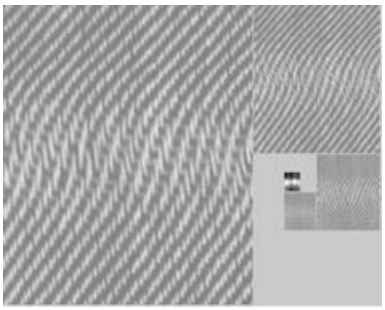

15(a)

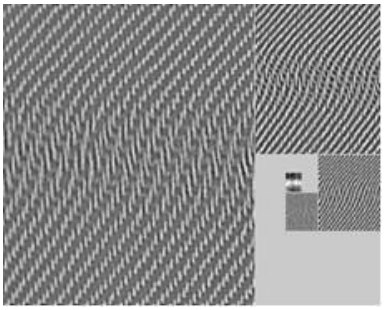

15(b)

Fig.15. (a) and (b) Gaussian and Laplacian Pyramids for Twill Fabric Image of Thin Place Defect

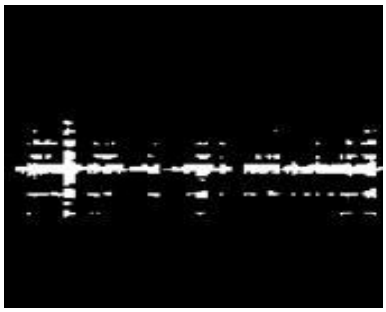

16(a) Gaussian

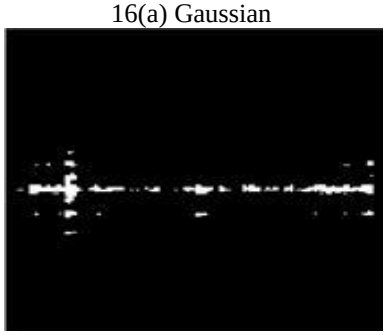

16(b) Laplacian

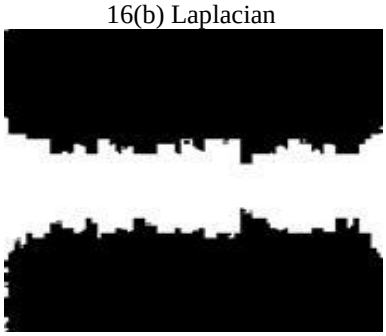

16(c) Steerable

Fig.16. (a)-(c) defect detection binary output image of pyramids of twill fabric image with thin place defect

5. CONCLUSIONS

One of the most important advantages of the method is that it is translation-invariance and scaled-invariance. This helps us to get the robust result for slight movement of the camera. The only considerations that require attention is number of pyramid levels to guarantee optimal performance, and a preliminary analysis of a prototype defect-free sample to extract the mean and standard deviation of its texture descriptors. The results of defect detection in fabrics shown and discussed in this paper lead - as first application - to textile inspection. Except for minor adaptations to each particular case, the method is ready to be used in an online industrial inspection system.

REFERENCES

[1] Ahmet Latif Amet, Aysin Ertuzun and Aytul Ercil, "An efficient method for Texture defect detection: Subband domain Co-occurrence Matrices", *Image and Vision Computing*, Vol. 18, No.6, pp. 543 – 553, 2000.

[2] Baykut A, Atalay A, Ercil A and Guler M, "Real-time defect inspection of textured surfaces", *Real-time Imaging*, Vol. 6, No. 1, pp. 17-27, 2000.

[3] Baykut A, Ozdemir S, Meylani R, Ercil A and Ertuzun A, "Comparative Evaluation of Texture Analysis Algorithms for Defect Inspection of Textile Products", *Proceedings of the 14th International Conference on Pattern Recognition (ICPR'98)*, Vol. 2, pp. 1738 – 1740, 1998.

[4] Chan C and Pang G., "Fabric Defect Detection by Fourier Analysis", *IEEE Transactions on Industry Applications*, Vol. 36, No.5, pp.1267 – 1276, 2000.

[5] E P Simoncelli and W T Freeman, "The Steerable pyramid: A flexible architecture for multiscale derivative computation", *International Conference on Image Processing*, Vol. 3, pp. 444 – 447, 1995.

[6] E P Simoncelli, W T Freeman, E H Adelson, and D J Heeger, "Shiftable multi-scale transforms", *IEEE Trans Information Theory*, Vol. 38, No. 2, pp. 587 – 607, 1992.

[7] Heeger D.J and Bergen J.R, "Pyramid-based texture analysis/synthesis", *Proceedings of Annual Conference on Computer Graphics and Interactive Techniques*, pp. 229–238, 1995.

[8] Jasper W. J, Garnier S and Potlapalli H, "Texture Characterization and defect detection using adaptive wavelets", *Optical Engineering*, Vol. 35, No. 11, pp. 3140-3149, 1996.

[9] Jasper W. J, Joines J. A and Brenzovich J, "Fabric Defect Detection Using a GA Tuned Wavelet Filter", *Proceedings of Computers and Their Applications*, pp. 345 – 350, 2003.

[10] Portilla J and Simoncelli E, "Texture modeling and synthesis using joint statistics of complex wavelet coefficients", *IEEE Workshop on Statistical and Computational Theories of Vision, Fort Collins, CO*, 1999.

[11] Kumar A and Pang G, "Fabric Defect Segmentation Using Multichannel blob detectors", *Optical Engineering*, Vol. 39, No. 12, pp. 3176 – 3190, 2000.

[12] Kumar A and Pang G, "Defect detection in textured materials using gabor filters", *IEEE Transactions on Industry Applications*, Vol. 38, No. 2, pp. 425 – 440, 2002.

[13] Miquel Rallo, Millan M S and Escofet J, "Wavelet based techniques for textile Inspection", *Optical Engineering*, Vol.26, No. 2, pp. 838 – 844, 2003.

[14] Burt P and Adelson E, "The Laplacian Pyramid as a Compact Image Code", *IEEE Transaction on Communications*, Vol. 31, No. 4, pp. 532 – 540, 1983.

[15] Sari-Sarraf H and Goddard J. Jr, "Vision system for on-loom fabric inspection", *IEEE Transactions on Industry Applications*, Vol. 36, No. 6, pp. 1252 – 1259, 1999.

[16] Tsai D M and Huang T Y, "Automated surface inspection for statistical textures", *Image and Vision Computing*, Vol.21, No. 4, pp. 307-323, 2003.

[17] Freeman W T and Adelson E H, "Steerable Filters", *in Topical Meeting on Image Understanding and Machine Vision, Optical Society of America, Technical Digest Series*, Vol. 14, 1989.

[18] Freeman W T and Adelson E H, "The Design and Use of Steerable Filters", *IEEE Transaction on Pattern Analysis and Machine Intelligence*, Vol. 13, No. 9, pp. 891 – 906, 1991.